Food Chemistry 518 (2026) 149680

Contents lists available at ScienceDirect

Food Chemistry

journal homepage: www.elsevier.com/locate/foodchem

Extraction mechanisms of proteins from *Palmaria palmata*

Agusman Agusman [a,1], Wouter J.J. Huijgen [a], Michel H.M. Eppink [b], Rene H. Wijffels [a,d], Norbert C.A. de Ruijter [c], Antoinette Kazbar [a,*]

[a] Bioprocess Engineering, Wageningen University & Research, Wageningen, PO Box 16, 6700 AA Wageningen, The Netherlands
[b] Bioprocess Engineering, TU Delft University, Building 58, room C2.150, Delft, The Netherlands
[c] Laboratory of Cell and Developmental Biology, Plant Sciences, Wageningen University & Research, PO Box 633, 6700 AP Wageningen, The Netherlands
[d] Faculty of Biosciences and Aquaculture, Nord University, Bodø N-8049, Norway

ARTICLE INFO

Keywords:
Palmaria palmata
Protein extraction
Tissue density
Microscopy
Cell wall
Xylanase
Alkaline extraction
Deep eutectic solvent

ABSTRACT

Protein extraction from *Palmaria palmata* remains challenging due to structural features that restrict protein release. This study evaluated alkaline solvents, xylanase enzymes, and deep eutectic solvents (DES) to assess protein recovery and structural changes using chemical analysis and microscopy. Protein yield, sugar solubilization, tissue density, protein localization, and cell wall integrity were examined. Microscopy revealed that proteins are concentrated in densely packed cortical cells with minimal intercellular space, limiting solvent penetration. Alkaline extraction achieved the highest protein recovery (~60%) with moderate structural disruption. Xylanase-assisted extraction caused greater cell wall breakdown but resulted in lower protein recovery (~27%), while DES treatment caused minimal disruption and yielded the lowest recovery (~14%). Carbohydrate solubilization did not correlate with protein recovery, indicating that cell wall degradation alone is insufficient. These findings identify dense cortical organization as a key constraint and highlight the need for combined mechanical and targeted biochemical strategies to improve extraction efficiency.

1. Introduction

The increasing global emphasis on sustainability in food production has heightened interest in valorizing plant-based products. Also, efficient recovery extraction of proteins from biomass is to meet global sustainability goals, aligning with several key objectives of the United Nations 2030 Agenda for Sustainable Development (*SDG 2: Zero Hunger, SDG 12: Responsible Consumption and Production, SDG 13: Climate Action, and SDG 14: Life Below Water*). In particular marine plant-based biomass has emerged as a promising resource to meet the rising demand for alternative proteins, anticipated to represent up to 20% of current soy protein production, with seaweed expected to play a major role in this growth (Janke, 2024; Yarish et al., 2016). Compared to terrestrial crops, seaweed cultivation requires minimal freshwater, fertilizers, or arable land, making it a potentially sustainable and efficient protein source (*Xie, & Yang, 2024*). Unlocking the full potential of seaweed protein through efficient extraction methods is thus critical for the development of marine-based biorefineries and for diversifying the protein supply chain. Among edible seaweeds, *P. palmata* (Rhodophyta; commonly known as dulse) has attracted attention due to its high protein content, up to 35% of its dry weight (Bjarnadóttir et al., 2018). Its unique bioactive properties and complete amino acid profile make it suitable for food, nutraceutical, and other applications (Machu et al., 2015; Sabeena & Jacobsen, 2013). Structurally, *P. palmata* has a relatively simple cell wall composition, primarily composed of 1,3- and 1,4-linked β-xylose, with smaller amounts of cellulose and galactose (Deniaud, Quemener, Fleurence, & Lahaye, 2003; Lahaye, Michel, & Barry, 1993).

Despite its potential, protein extraction from *P. palmata* is currently inefficient, resulting in low yields and leaving significant amounts of protein in the residual biomass (Liu et al., 2024). Structural barriers, such as resilient polysaccharide matrices and tightly bound protein–cell wall associations, hinder efficient protein release, presenting a bottleneck in biorefinery workflows (Aslam, Akhtar, Nazir, Khalid, & Barrow, 2024). Generally, extraction processes follow three steps: size reduction (enhancing solvent accessibility) (Bojorges, López-Rubio, Martínez-Abad, & Fabra, 2023), extraction (using chemical, enzyme-assisted, or combined methods), and separation of the extract from remaining solids.

Several approaches have been studied for protein extraction. Among the chemical approaches, alkaline extraction remains the most widely

* Corresponding author.
[1] National Research and Innovation Agency of Indonesia, Jl. M.H. Thamrin No. 8, Central Jakarta, Jakarta, 10340, Indonesia.

https://doi.org/10.1016/j.foodchem.2026.149680
Received 10 November 2025; Received in revised form 26 February 2026; Accepted 15 May 2026
Available online 17 May 2026

used, as it enhances protein solubility by disrupting polysaccharide structures, increasing sugar solubilization, and hydrolyzing peptides into shorter chains (Hadidi, Aghababaei, & McClements, 2023; Juul, Haue, Bruhn, Boderskov, & Kastrup Dalsgaard, 2023; Vilg & Undeland, 2017; Wang et al., 2025). Alkaline extraction has been reported to recover 45–61% of the total protein content of *P. palmata* (Harnedy & FitzGerald, 2013; Naseri, Marinho, Holdt, Bartela, & Jacobsen, 2020). Enzyme-assisted extraction using xylanase to hydrolyze the major components of the cell wall matrix has also been studied; however, this method recovers only about 25% of the total protein (Bjarnadóttir et al., 2018). Finally, deep eutectic solvents (DES), a class of emerging green solvents capable of disrupting hydrogen bonding networks, have shown potential for improving cell wall decomposition, though subsequent protein extraction yields remain low (~14%) with this method (Hernández-Corroto, Olivares-Galván, Marina, & García, 2023; Liu et al., 2017; Moldes et al., 2024; Shawky, Zhu, & Tian, 2025).

Previous studies employed trial-and-error approaches such as extended processing times, increased enzyme concentrations, multi-enzyme cocktails, or hybrid alkaline-enzyme treatments to increase protein extraction efficiency (Harnedy & FitzGerald, 2013; Naseri et al., 2020). However, the fundamental mechanisms limiting protein release from *P. palmata* remain poorly understood. A critical challenge in microstructural and compositional features of seaweed tissues has largely been overlooked. Unlike land plants, seaweeds exhibit distinct cellular architectures and structural organization reflecting their separate evolutionary paths and adaptations to different environments. Understanding these structural differences will help in developing optimum processes for protein extraction.

Microscopy can provide valuable insights into these structural barriers. Techniques such as light microscopy and electron microscopy enable visualization of cell-wall architecture, with which tissue integrity and protein distribution can be studied. These observations help identify cellular structures that hinder extraction and guide the development of more effective, targeted extraction strategies. To date, few studies have been reported where microscopy and chemical analyses were integrated to investigate extraction processes. One example is a study conducted by Wijethunga, He, Prithiviraj, and Sun (2025), where light and electron microscopy were used to observe the effects of acid and microwave treatments on protein extraction from the thallus of *P. palmata*. However, that study only depicted changes at the surface of the thallus (epidermis). Structural analysis of biomass generates valuable information when combined with protein localization, compositional profiling, and extraction yield data, allowing for a deeper understanding of the relationship between tissue disruption, carbohydrate release, and protein extraction yield.

This study aims to elucidate the protein extraction process from *P. palmata* by combining microscopy with chemical analyses. Three extraction strategies (alkaline, enzyme-assisted, and DES-based) were studied. Both initial biomass and extraction residues were analyzed using specific staining techniques combined with advanced light microscopy. Protein recovery yield and carbohydrate released were quantified to investigate correlations between cell wall disentanglement, protein localization, and extraction efficiency. This integrated approach provides mechanistic insights into protein accessibility at the cellular level, offering a foundation for optimizing protein recovery yield from seaweed.

2. Methodology

The methodology was designed to obtain both liquid extracts (supernatants) and solid residues from different extraction treatments, enabling quantification of protein and carbohydrates while also assessing tissue structure through microscopy. All extraction treatments were performed on the same batch of dried and size-reduced *P. palmata* to ensure comparability.

2.1. Biomass and sample preparation

Fresh tank-cultured *P. palmata* was obtained from Hortimare BV (The Netherlands) and transported on ice. Biomass was rinsed briefly with tap water to remove surface salts and air-dried in a fume hood for 48 h. A single batch of harvested biomass comprised multiple gametophytes. The dried material was flash-frozen using liquid nitrogen and manually ground with a mortar and pestle. The size-reduced biomass was stored at 4 °C until extraction. A portion of fresh biomass was acclimated in f/2 medium at 10 °C for 48 h prior to fixation and resin embedding.

2.2. Extraction procedures

Three extraction strategies were evaluated: xylanase-assisted extraction (enzymatic), alkaline extraction, and extraction using a deep eutectic solvent (DES). All experiments were performed in 15 mL centrifuge tubes unless otherwise stated.

2.2.1. Enzyme-assisted extraction

A modified protocol based on Fleurence, Massiani, Guyader, and Mabeau (1995) was used. Xylanase (2500 U/g, Sigma Aldrich X2753) was dissolved in sodium oxalate buffer (pH 6) to obtain a 4 U/mL solution. Approximately 100 mg of dried biomass was mixed with 10 mL enzyme solution, vortexed for 30 s, and incubated at 55 °C for 24 h with shaking (180 rpm). Samples were centrifuged at 4800 rpm for 15 min; supernatants were frozen at −20 °C, while residues were washed twice with Milli-Q water and stored at 4 °C.

2.2.2. Alkaline extraction

Following Harnedy and FitzGerald (2013) with modifications, 100 mg of dried biomass was mixed with 10 mL of 0.2 M NaOH and vortexed for 30 s. The mixture was incubated at 60 °C for 6 h while shaking (180 rpm). Centrifugation and washing steps followed the procedure in Section 2.2.1.

2.2.3. DES-assisted extraction

A betaine:urea:water DES (1:2:1 M ratio) was prepared following Moldes et al. (2024). For each extraction, 250 mg biomass was mixed with 2.25 mL DES, vortexed briefly, and incubated at 30 °C for 3 h with manual stirring every 30 min. Samples were centrifuged to separate residue and extract. Extracts were stored at 4 °C and residues were washed and stored as described above.

2.3. Protein quantification

Total protein content of dried biomass was determined using the Dumas combustion method (Rapid N exceed, Germany). Protein in enzymatic and alkaline extracts was quantified using TOC/TN analysis (Shimadzu, Japan), applying a nitrogen-to-protein conversion factor of 4.7 (Bjarnadóttir et al., 2018). Protein recovery yield was calculated as the ratio of protein in extract to total protein in starting biomass (% *w/w*). Protein in DES extracts was quantified via the Bradford assay due to matrix incompatibility with TOC/TN analysis, as urea is falsely measured as nitrogen and can lead to an overestimation of protein content. The Bradford method has been used for quantifying protein in DES extracts (Moldes et al., 2024).

2.4. Carbohydrate analysis

Extracted carbohydrate was measured by hydrolyzing 100 μL of extract using concentrated sulfuric acid following a modified NREL protocol (Van Wychen & Laurens, 2023), followed by HPAE-PAD monosaccharide analysis (Dionex ICS 6000, CarboPac PA20 column). Monosaccharide concentrations were quantified against standard calibration curves and expressed as μg sugar per mg biomass (dry basis).

2.5. Microscopy and image analysis

2.5.1. Sample fixation and embedding

Fresh and extracted tissues were fixed in 4% paraformaldehyde solution containing glutaraldehyde, PIPES buffer, Triton X-100, and DTT. To ease sample processing and tissue positioning these thallus strips or extracted biomass samples of approximately 200 mg were flat oriented in 1 mL of melted 4% low-melting point (LMP) agarose (Invitrogen 16,520,100, UltraPure™) at 27 °C and allowed to solidify in the fridge. After LMP agarose embedding, samples were dehydrated through a graded ethanol series, infiltrated with Technovit 7100 resin, and polymerized at 37 °C (Matsushima, 2014). Sections of 5 μm thickness were obtained using a Leica RM2145 microtome and stretched on water surface prior to glass mounting and staining.

2.5.2. Staining and imaging

Toluidine Blue (TB) was used to visualize acidic tissue (protein-rich) regions, Hoechst 33342 to stain nuclei, and Calcofluor White (CFW) to detect all β -(1,3) and β-(1,4)-linked polymers. Brightfield images (TB) and (Hoechst, CFW) were acquired using a Nikon 80i microscope, while fluorescence CFW was acquired using a Stellaris 5 Confocal LSM Leica. The sample preparation, staining, washing times, and mounting were standardized. Also, image acquisition was performed under standardized excitation, gain, and exposure settings to meet criteria for intensity comparison.

2.5.3. Quantitative image analysis

Regions of interest (cortex–medulla–cortex) were defined in ImageJ (Fiji 1.54p). TB and CFW intensities were normalized to a 0–100% scale. Nuclear counts were determined from thresholded Hoechst images. Signal intensity was quantified from three randomly chosen in-focus image planes of multi-sections (2–3) mounted on a microscopy slide. Field-to-field variability within the same sample was estimated by calculating the standard deviation across three images. The schematics for data analysis are shown in **Fig. S1–3.** The intercellular space (ICS), i.e., the void space between cells, was measured from CFW-stained images of intact thallus/tissues. The void areas were selected using the Cell Magic Wand tool in ImageJ. A total of 96 intercellular spaces were measured from 3 images for the medullary domain and the cortical domain. Cell size was measured by manually tracing the outer boundary of the cell wall using the freehand selection tool; a total of 110 cells were quantified across three randomly chosen CFW-stained image planes. Meanwhile, cell size in the epidermis (surface) is measured from fresh, unstained brightfield images. The cell wall thickness was measured using Local Thickness analysis of a masked image (converted to binary) from a single image plane.

2.6. Statistical analysis

One-way ANOVA ($p < 0.05$) was used to assess differences across extraction methods and control. Pearson correlation was applied to evaluate relationships between sugar solubilization and protein recovery.

3. Results and discussion

In this section, we first evaluate the effectiveness of alkaline extraction, enzyme-assisted extraction, and DES treatment for isolating protein from *P. palmata*. The tissue architecture of the intact *P. palmata* thallus is described. Subsequently, we present microscopic analyses of the extraction residues to assess changes in acidic components (tissue presence), cell density, cell wall structure, and their spatial distribution at a cross-section. Additionally, the extracted sugars, galactose, glucose, and xylose, are discussed to elucidate the relationship between protein recovery yield and cell wall disruption.

3.1. Protein recovery yield of alkaline, enzymatic, and DES extraction

Protein recovery yields differed substantially among the extraction strategies (Table 1). The alkaline extraction resulted in the highest protein recovery yield (60.4 ± 3.1%), which is consistent with previously reported values of 45–61% obtained using NaOH-based extraction (Harnedy & FitzGerald, 2013; Idowu, Amigo-Benavent, & FitzGerald, 2024; Naseri et al., 2020). This confirms that alkaline extraction serves as an effective benchmark for *P. palmata* protein recovery and remains the reference process in biorefinery workflows.

Enzyme-assisted extraction using xylanase recovered 26.7 ± 0.8% of the total protein, which is in line with earlier findings reporting protein recoveries of approximately 25% (Bjarnadóttir et al., 2018). Xylanase effectively hydrolyzes xylan, the dominant hemicellulosic component of the *P. palmata* cell wall. However, the breakdown of this major polysaccharide did not proportionally improve protein solubility or recovery yield. This observation is consistent with prior reports stating that enzymatic hydrolysis of the cell wall alone does not sufficiently release cytoplasmic proteins that remain embedded within densely packed tissues (Aasen, Sandbakken, Toldnes, Roleda, & Slizyte, 2022).

The DES-based extraction (betaine:urea:water, 1:2:1 M ratio) yielded the lowest protein recovery (14.4 ± 6.7%). This low efficiency aligns with earlier studies on *Saccharina latissima* and *Ulva* spp., where DES treatments primarily facilitated limited carbohydrate solubilization but did not effectively liberate intracellular proteins (Liu et al., 2017; Moldes et al., 2024; Shawky et al., 2025). The relatively low protein yield observed in this study may be associated with insufficient penetration of the DES into structurally dense cortical regions, combined with limited disruption of protein-polysaccharide interactions.

Overall, alkaline extraction achieved the highest protein recovery (~60%), followed by enzyme-assisted extraction (~27%) and finally DES-based extraction (~14%). These differences emphasize that protein recovery is governed not only by cell wall disentanglement, but also by the ability of the extraction method to solubilize and mobilize intracellular proteins from compact thallus tissues.

It should be noted that protein concentrations in DES extracts were quantified using a different analytical method (Bradford assay) than that used for alkaline and enzymatic extracts (TOC/TN), which should be taken into account when comparing absolute protein values across extraction systems. Nevertheless, the comparison of the protein extraction yields remains relevant for the present study. Previous studies have reported that Bradford quantification can be approximately 20% lower than values obtained by micro-Kjeldahl analysis, using nitrogen-to-protein conversion factors, in maize protein samples, because Kjeldahl quantifies total protein while Bradford detects only soluble, dye-binding proteins (Kaur et al., 2022; Kruger, 1994; Noble & Bailey, 2009). Therefore, considering the potential underestimation associated with the Bradford method, the observed protein extraction yield (14%) in DES extracts can still be reasonably used for comparative evaluation of

Table 1
Protein extraction efficiency of different extraction approaches from *P.palmata.*

Extraction method	Conditions			Time (h)	Protein recovery yield (%)
Alkaline	Solvent	:	0.2 M NaOH in water		
	Temperature	:	60 °C	6	60.4 ± 3.1
Enzymatic	Solvent	:	3 unit/mL xylanase in sodium oxalate buffer		
	Temperature	:	50 °C	24	26.7 ± 0.8
DES	Solvent	:	1 betain: 2 urea: 1 water at a molar ratio		
	Temperature	:	30 °C	3	14.4 ± 6.7

extraction performance, while acknowledging methodological differences between quantification approaches.

3.2. Structural Organization of the Intact P. palmata thallus

P.palmata is a foliose red alga with a tough, flat, leathery frond and a fleshy and flexible skin-like texture, shown in Fig. 1a. Fig. 1b shows the brightfield image of the thallus surface of fresh unstained tissue, which is assembled by tightly enclosed, relatively similar-sized cells. Fig. 1c-e shows a cross-section of a freshly fixed and resin-embedded *P. palmata* thallus blade after TB and CFW staining. The histological staining revealed clear anatomical differentiation between cortical and medullary regions in *P. palmata* thallus. TB staining (Fig. 1c) shows a tight organization of dense small cells in a cortical peripheral layer that surrounds a medullary inner region with large cells and thicker walls. In addition to their larger size, cells in the medullary region frequently contained a prominent central vacuole, visible as unstained or weakly stained regions within the cytoplasm in both TB and CFW (green arrow in Fig. 1c). The longitudinal section image of the fresh thallus confirmed the bigger cell in the medulla contained a central vacuole **(Fig. S4a)**. This cell differentiation proved that studying the surface layer (epidermis) alone is insufficient to explain the tissue changes observed during the extraction process.

The variation in cell size in a cross-section and epidermis is shown in **Fig. S4b**. Note these volumes are an underestimation, since we only measured cross-sections. A dense tissue organization of *P. palmata* was also observed by CFW fluorescence imaging, which allowed visualization of cell walls and quantitative morphometric analysis of cellular parameters (Fig. 1d–e). We observed cell contact, i.e., cell wall area where two adjacent cells connected (as indicated by the white arrows). We used a bigger intercellular space (ICS) between cells as an indicator for lower cellular connectivity. We found compact tissue arrangements with minimal ICS in the cortical region, in contrast to the more open architecture of the medullary region. The violin plot analysis of ICS distribution revealed apparent differences in cell connectivity between two domains (Fig. 1f**).** In the cortical region, ICS areas were right-skewed, with most measurements clustering near zero (mean: 12.42 $\pm$ 9.78 μm^2), indicating that most cortical cells have small or negligible ICS. Conversely, the medullary region exhibited a broad, symmetrical distribution (mean: 93.56 $\pm$ 53.77 μm^2) with greater variability and larger ICS, extending up to ~200 μm^2. Taller and wider violin shape, reflecting a higher proportion of cells with expanded ICS.

We also attempted to examine the ICS in epidermal or flat fronds of CFW-stained fresh tissue; however, we were unable to measure it due to its small size **(Fig. S4c).** We highlight the ICS, as it explains how solvents penetrate the inner tissues. The extraction solvent has better access to the inner tissues from the medulla region than from the cortical regions and epidermis, as the medulla region has a larger ICS (less cell contact) than the cortex and epidermal regions. The ICS was also stained by TB (Fig. 1c), as pointed by the orange arrow, possibly because part of the ICS of *P.palmata* may be filled with acidic mucilage and water (as indicated by the white arrows Orange arrow in Fig.1c). In the inner cortex of *Rhodymenia* (a red seaweed), the cells are arranged irregularly, and the ICS are occupied by mucilage (Baweja, Kumar, Sahoo, & Levine, 2016).

Cell wall thickness mapping using CFW-stained images revealed significant spatial heterogeneity in the cell wall of *P. palmata* (Fig. 1g). The cell in the cortex exhibited consistently thin walls and cool-colored zones on the heatmap. In contrast, cells in the medulla showed thicker walls, indicated by warmer orange-red zones. The transition zone exhibited a gradual increase in thickness. A violin plot (Fig. 1h) demonstrated these differences, with cortical wall thickness (mean: 3.75 $\pm$ 1.72 μm) showing low variability, while medullary walls (mean: 6.96 $\pm$ 3.08 μm) had greater variability and a wider range. However, the cell wall thickness might be proportional to cell size, as the cell size also varies.

3.3. Analysis of extraction efficiency using toluidine blue staining on cross-sections of tissue residues

3.3.1. Overall tissue intensity on extraction residues

Toluidine Blue (TB) staining was applied to visualize acidic tissue (proteins) and polysaccharides and to compare the extracted biomass residues with the untreated control biomass processed under identical embedding and imaging conditions. As shown in **Fig. S5**, the control biomass (**Fig. S5a**) exhibited a deep blue coloration, whereas the extracted residues showed progressively paler staining intensities depending on the extraction treatment (**Fig. S5b–d**). Because all samples were stained, destained, and imaged under standardized conditions, these differences in staining intensity reflect genuine depletion of acidic cellular components during extraction, rather than artifacts of sample preparation. TB is a thiazine metachromatic dye with strong affinity toward acidic tissue constituents, including proteoglycans and glycosaminoglycans (Sanchez et al., 2001). Dissolving TB in boric acid (pH 4) further enhances dye binding affinity to samples with different treatment histories (Sasaki & Matsui, 1972; Sridharan & Shankar, 2012).

Despite chemical treatments, most extracted residues retained an overall intact tissue morphology (**Fig. S5b–d**), indicating that none of the extraction methods fully disrupted the cellular structure or completely released intracellular content. This is consistent with the observation of dense blue-stained cytoplasmic regions surrounded by distinct, unstained cell walls (Fig. 1c**; Fig. S5a**). Although chloroplast pigments such as phycoerythrin can be partially removed by ethanol during resin embedding (Bouzon, Simioni, & Schmidt, 2014), the acidic glycoprotein-rich cytoplasm remains and is therefore strongly stained by TB. By contrast, extensive protein release would be expected to result in loss of cytoplasmic staining and visible collapse or fragmentation of cells, which was not observed here.

Quantitative comparison of overall TB signal intensities (Fig. 2a) confirmed a significantly higher ($p < 0.05$) staining intensity in the control biomass compared to all extracted residues. Among treatments, alkaline extraction produced the lowest TB intensity, indicating a greater loss of acidic cellular components relative to enzymatic and DES-assisted extraction. Interestingly, enzymatic and DES residues exhibited similar TB intensities, despite their markedly different protein recovery yields. This discrepancy may arise from the use of the Bradford assay for DES extracts, which may underestimate protein concentration in the presence of betaine and urea, as discussed in section 3.1.

3.3.2. Cellular density distribution along the thallus cross-section

The preservation of overall tissue architecture in extracted residues enabled spatial analysis of TB staining across the cortex–medulla–cortex (CMC) cross-section. In the untreated biomass (Fig. 2b), TB intensity followed a characteristic U-shaped profile, with stronger staining in the cortical regions and weaker staining in the medulla. This profile reflects a higher concentration of protein-rich, photosynthetically active small cells in the cortex, whereas the medullary region consists of larger cells with lower cytoplasmic density. Similar spatial distributions of protein-rich cortical tissue have been reported in other red and green macroalgae, including *Porphyra umbilicalis* and *Ulva lactuca*, where photosynthetic pigments and phycobiliproteins are concentrated in peripheral cell layers (Karina et al., 2022; Ramus, Beale, Mauzerall, & Howard, 1976). The present study provides the first direct microscopic evidence that protein in *P. palmata* is predominantly localized in the cortex.

In all extracted residues, the U-shaped intensity profile persisted but was uniformly shifted downward (Fig. 2c), indicating removal of acidic components from both cortical and medullary tissues. However, the medullary region appeared more extractable than the cortex, likely due to larger intercellular spaces (ICS) facilitating solvent diffusion, whereas the dense cortical tissue with tightly packed cells and minimal ICS, acted as a diffusion barrier. Additionally, larger medullary cells may be more readily disrupted during cryogenic size reduction. These findings align with previous observations that phycobiliproteins dominant in cortical

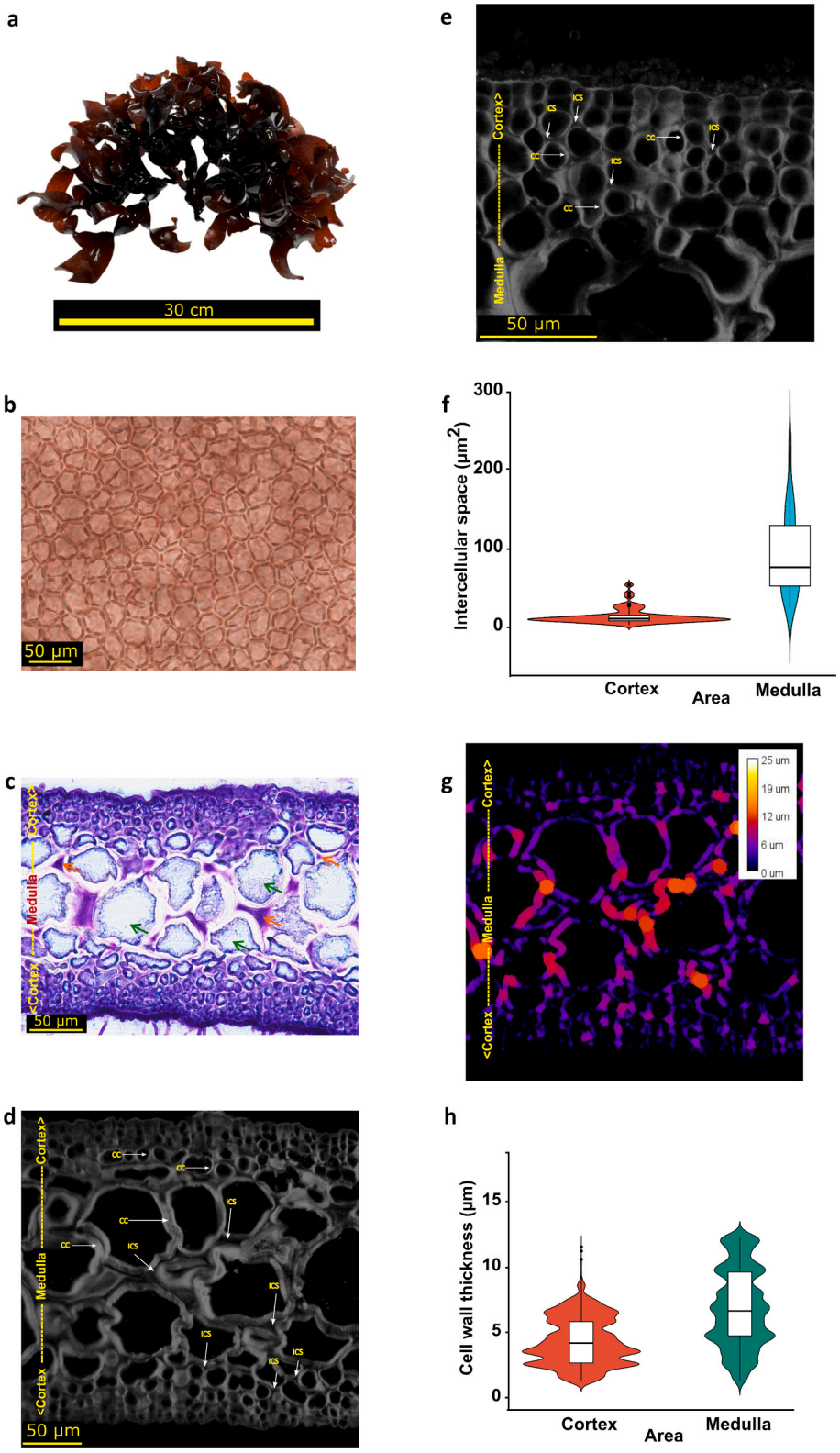

Fig. 1. (a) Habitus of *P.palmata* thallus. (b) Thallus surface of fresh unstained tissue. Cross planes of embedded intact tissues of *P.palmata* (c) with toluidine blue staining. (d) with calcofluor white staining in medulla region and (e) with calcofluor white in cortical region. Green arrows indicate vacuoles (Fig. 1c), white arrows indicate cell contact (CC) or intercellular space (ICS). (f) Intercellular space area in cortex and medulla. (g) Overview of cell wall thickness. (h) Cell wall thickness in cortex and medulla. (For interpretation of the references to colour in this figure legend, the reader is referred to the web version of this article.)

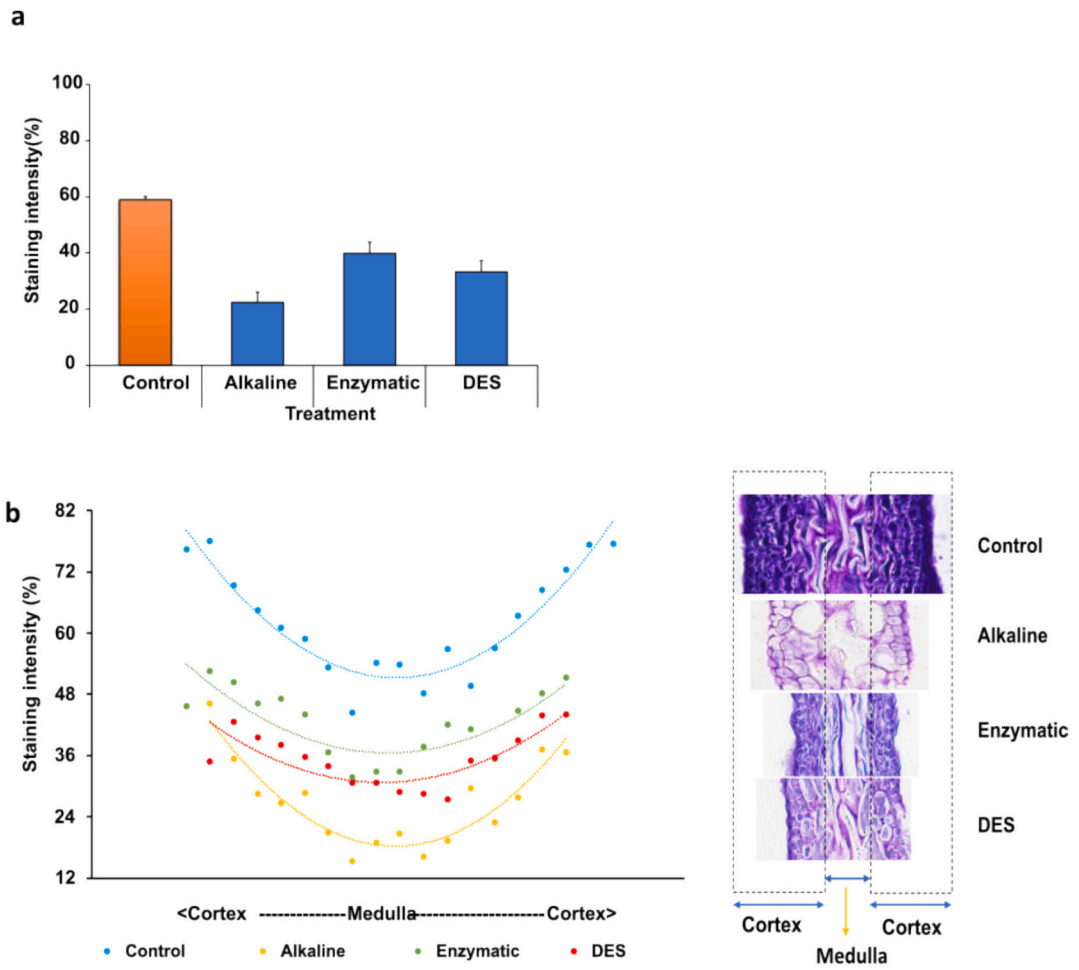

Fig. 2. (a) Overall Toluidine Blue (TB) staining intensity of residues. Significant differences compared with the control are indicated by different bar colors. (b) TB distribution of treated biomass at a cross-section from cortex-medulla-cortex. The distribution of CFW intensity was generated from three image planes of each treatment. (For interpretation of the references to colour in this figure legend, the reader is referred to the web version of this article.)

regions are more difficult to extract (Garbary & Kim, 2005; Lüder, Knoetzel, & Wiencke, 2001).

Alkaline extraction, which yielded the highest protein recovery (60%, Table 1), resulted in pronounced loss of TB signal in the medulla (Fig. 2b) and reduced cytoplasmic staining overall. However, the persistence of structural protein-rich cell walls suggests that additional enzymatic or combined treatments are required for further improvement. Indeed, synergistic alkaline–xylanase–cellulase combinations have previously been shown to enhance protein recovery to ~70% (Idowu et al., 2024; Mæhre, Jensen, & Eilertsen, 2016). These observations support the interpretation that ~60–70% represents a practical upper recovery limit for alkaline extraction alone.

3.4. Cellular density in P. palmate probed with nuclei staining

3.4.1. Tissue density of treated thallus

Tissue density is a characteristic of biomass that influences the extraction process. High tissue density leads to reduced solvent diffusion, slowing the transfer of the solid matrix to the liquid solvent (Zhao, Wang, & Huang, 2024). In this study, the nucleus was probed using Hoechst 33342 staining in vertical cross sections (CMC) of *P. palmata* to count the number of cells. Fig. 3a shows the nucleus of the embedded section of intact tissue of *P. palmata* at a cross-section. It shows more nuclei in the cortical region than in the medullary region, confirming TB and CFW results. This pattern was also found in treated biomass (**Fig. S6**). Fig. 3b shows an apparent variation in tissue density of the treated biomass against the control biomass. Notably, statistical analysis revealed no significant differences ($p > 0.05$) in cellular density between the initial biomass and treated biomass, indicating that treatments did not alter cell density. The lower average cell count in the alkaline and enzymatic treatments suggests that the extraction solvents penetrated the cytoplasm, which degraded the nucleus or interrupted the binding of Hoechst 33342 to the nucleus. DES treatment results, with a relatively high average nucleus count compared to alkaline and enzymatic treatments, indicate less contact or solvent penetration to cytoplasm compared to alkaline and enzymatic treatments.

Moreover, similar thallus densities across treatments and differing protein recovery yields suggest that the extraction mechanisms vary among the processes. Under alkaline conditions, protein solubility also increases, as the treatment breaks down proteins into smaller fragments, facilitating more effective transfer from solid tissue to the solvent. The alkaline treatment resulted in a smaller protein subunit during the extraction of protein from *Pyropia seriata* (Zhang et al., 2024). Extraction solvents were unable to significantly reduce the tissue density, which limited the extraction of the protein from *P. palmata*. Dense tissue leads to reduced solvent penetration due to the increased resistance and limited space for solvent molecules to diffuse (Brglez Mojzer, Knez Hrnčič, Škerget, Knez, & Bren, 2016; Yadav & Singh, 2020). High cell density not only hinders the extraction of targeted products in the cytoplasm but also affects the cell wall disruption (Wang et al., 2024).

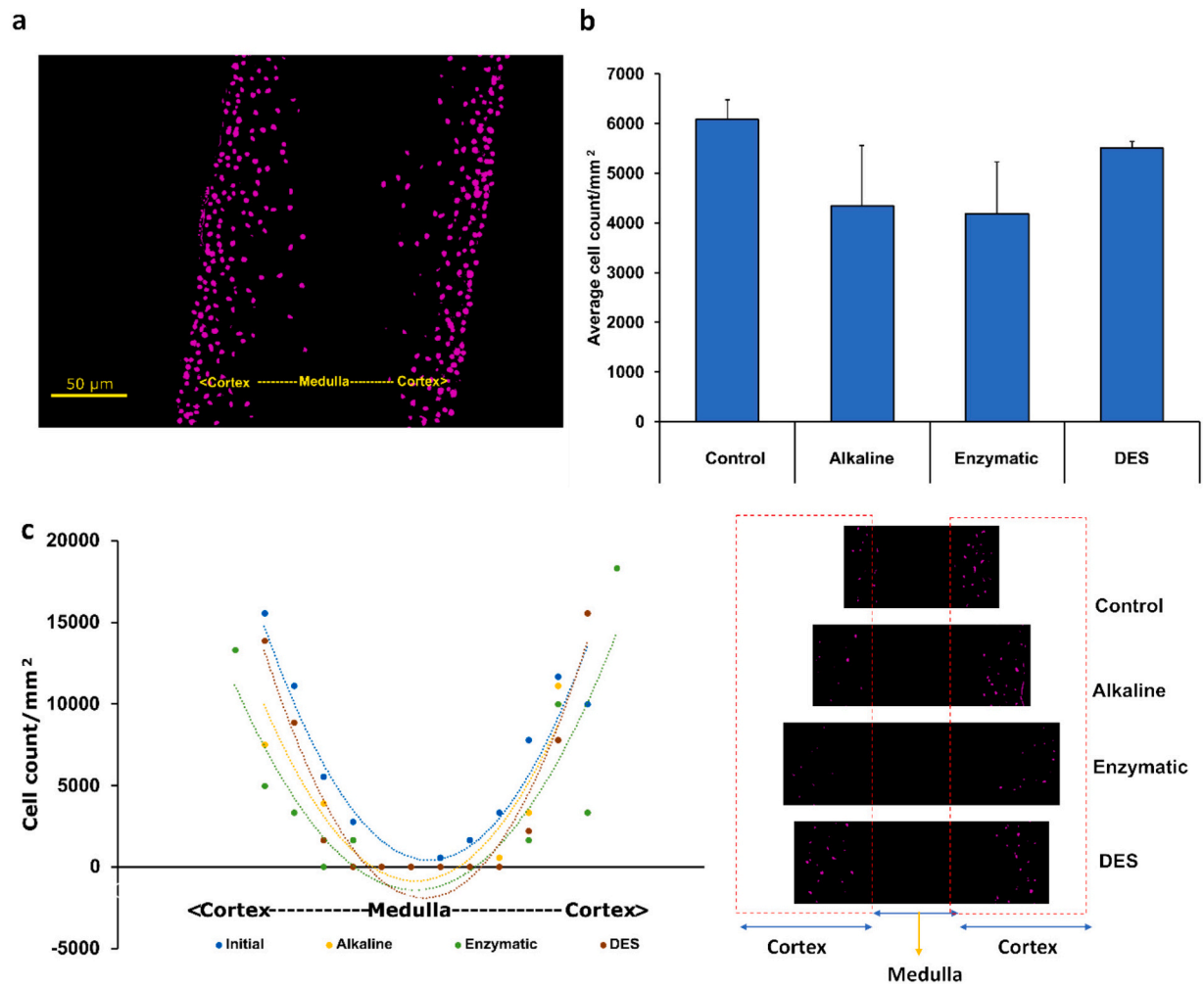

Fig. 3. (a) Stained nuclei in untreated thallus of *P.palmata.* (b) Average cell count/mm^2 of control and extracted thallus. (c) Distribution of cell count/mm^2 (tissue density) over vertical cross-sections based on Hoechst 33342 staining of the nuclei. The distribution of CFW intensity was generated from three image planes of each treatment.

3.4.2. *Spatial distribution of cells from cortex to medulla*

Spatial distribution of cell count/mm^2 (cell density) in the vertical cross-section of *P. palmata* thallus, extending from CMC, is illustrated in Fig. 3c. The cell distribution of the initial biomass exhibited a pronounced U-shape, and this distribution remained unchanged after extraction. Despite the treatments, there is no strong tissue collapse or shrinkage visible as a result of the embedding process. Prior to the embedding procedure, tissue residues were aldehyde-fixated and not affected morphologically anymore. This was confirmed by a similar cell count of epidermis cells per 100 µm of fresh tissue and embedded section tissues (**Fig. S7**).

The dense tissue within the cortical region is noteworthy in the biorefinery process, as these areas contain a higher concentration of proteins, as indicated by the TB signal. However, packed cells within tissues present a challenge for protein recovery. High tissue density, with tight cell connections in a tissue, like smaller intercellular spaces, can limit solvent entry to mediate extraction. In addition, the inner thallus (cortical and medullary region) is also protected by the epidermal layer (outer layer), which has a higher cell density (10,954.85 ± 559.7366 cell/mm^2, count from image Fig. 1b) compared to the average cell density of the control biomass at cross-section. This finding suggests that those areas rich in protein are well protected by the morphological architecture of *P. palmata*. Therefore, implementing an effective strategy to deal with dense tissues/biomass to facilitate solvent penetration is suggested to enhance protein extraction from *P. palmata*. This strategy can be applied during the biorefinery process (downstream) and/or during biomass cultivation (upstream).

Process note. Extraction performance is thus constrained by tissue density and solvent access (Brglez Mojzer et al., 2016; Yadav & Singh, 2020; Zhao et al., 2024), while alkaline conditions additionally contribute via peptide cleavage and increased solubility (Zhang et al., 2024), and cell wall degradation can also be impacted by density effects (Wang et al., 2024).

3.5. *Cell wall alteration of P. palmata during the extraction process*

Spatial cell wall degradation was evaluated based on the loss of CFW fluorescence intensity in the extraction residues. The cell wall of *P. palmata* consists predominantly of mixed-linkage β-(1,3)/β-(1,4)-D-xylans, with smaller amounts of β-(1,4)-D-xylans and cellulose (Deniaud et al., 2003). These polysaccharides can be visualized using CFW, which binds specifically to β-(1,3)- and β-(1,4)-glucans (Piccinini, Nirina Ramamonjy, & Ursache, 2024). The specificity of CFW for β-(1,4)-xylose was confirmed using purified beechwood xylan (**Fig. S8**).

CFW interacts with β-(1,4)-linked polysaccharides such as cellulose, which forms linear, rigid, and largely insoluble fibrillar networks contributing to cell wall structural integrity. Owing to its high affinity and strong fluorescence, even low amounts of β-linked polysaccharides can be readily detected. However, the probe is non-stoichiometric, and its fluorescence intensity is influenced by polysaccharide accessibility,

cell wall architecture, and staining conditions. Therefore, the signal does not directly correspond to the absolute polysaccharide content. When samples are processed and imaged under identical conditions, CFW fluorescence can be interpreted in a semi-quantitative manner for relative comparison between similar samples.

Importantly, because CFW broadly binds to β-(1,3)- and β-(1,4)-linked polysaccharide networks, including cellulose and xylans, it cannot discriminate between specific cell wall components or distinct wall layers that may be differentially affected by processing. Consequently, changes in CFW intensity should be interpreted as an indication of overall alterations in the organization of β-polysaccharide structures rather than precise compositional or localized structural modifications of individual cell wall polymers.

Fig. S9 shows CFW-stained cross-sections of control and extracted biomass. CFW signal was present in both cortical and medullary regions, although differences in brightness may reflect variations in the composition or accessibility of cellulose versus xylan. Quantification of total CFW signal (Fig. 4) revealed significantly higher fluorescence in the control biomass ($p < 0.05$), confirming that all extraction treatments induced some degree of cell wall alteration.

Among treatments, the enzymatic (xylanase) extraction resulted in the lowest CFW signal, indicating the most severe cell wall degradation as result of xylanase hydrolyzing the dominant wall polysaccharide (Zhao et al., 2023). In contrast, DES-treated residues exhibited the highest remaining CFW signal, indicating the least cell wall disruption. Alkaline-treated residues showed intermediate signal levels.

Spatial distribution of the CFW signal across the cortex–medulla–cortex plane (Fig. 4b) demonstrated that the medullary region consistently exhibited higher CFW intensity than the cortex, suggesting a more robust or less extractable wall architecture. Following xylanase treatment, the medulla retained strong CFW fluorescence, suggesting that cellulose may be more abundant or less accessible there, as xylanase hydrolyzes only xylan but not cellulose. Further work employing xylan- and cellulose-specific monoclonal antibodies could clarify the localization of cell wall polymers.

Interestingly, the extent of cell wall degradation did not correlate with protein recovery yield. Xylanase caused the greatest loss of CFW signal but recovered only ~27% protein, whereas alkaline extraction caused only moderate cell wall degradation yet achieved ~60% protein recovery (Table 1). DES extraction resulted in minimal cell wall alteration and the lowest protein recovery (~14%).

Prior study showed that acid hydrolysis and microwave-assisted treatments reduced CFW signal and generated higher protein extraction yield (Wijethunga et al., 2025). However, in same paper, authors did not depict the effect of multi-enzyme treatment (e.g., Viscozyme, containing cellulase, β-glucanase, hemicellulase, and xylanase) on CFW signal nor how protein recovery relates to cytoplasmic protein size and tissue packing. Our results, together with earlier reports, indicate that cell wall disruption alone is insufficient for efficient protein release. Instead, protein solubilization possibly due to peptide cleavage, such as under alkaline conditions, appears to be a key factor enabling cytoplasmic protein mobilization. Thus, cell wall breakdown and protein solubilization act as complementary, not interchangeable, mechanisms in the extraction process.

3.6. Cell wall degradation as indicated by dissolved sugar

To further assess cell wall degradation, the extracts were hydrolyzed and analyzed for glucose, galactose, and xylose (Fig. 5a). The sugar profiles confirmed that xylanase-assisted extraction caused the highest release of monosaccharides, followed by alkaline extraction and then DES extraction.

Enzyme-assisted extraction showed the highest release of xylose (764 μg/mg biomass d.b.), along with lower amounts of galactose (44

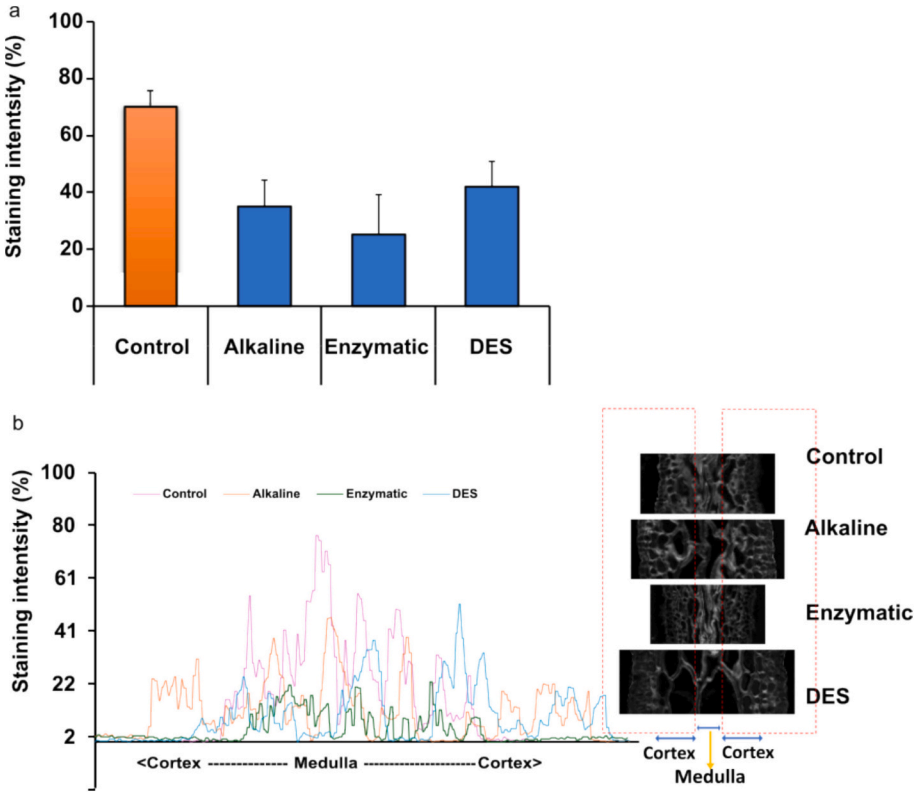

Fig. 4. (a). Overall calcofluor white staining intensity on treated biomass. Significant differences compared with the control are indicated by different bar colors. (b) Calcofluor white staining intensity distribution over (treated) biomass at cross-sections from cortex-medulla-cortex (normalized for length). The distribution of CFW intensity was generated from a single plan of each treatment.

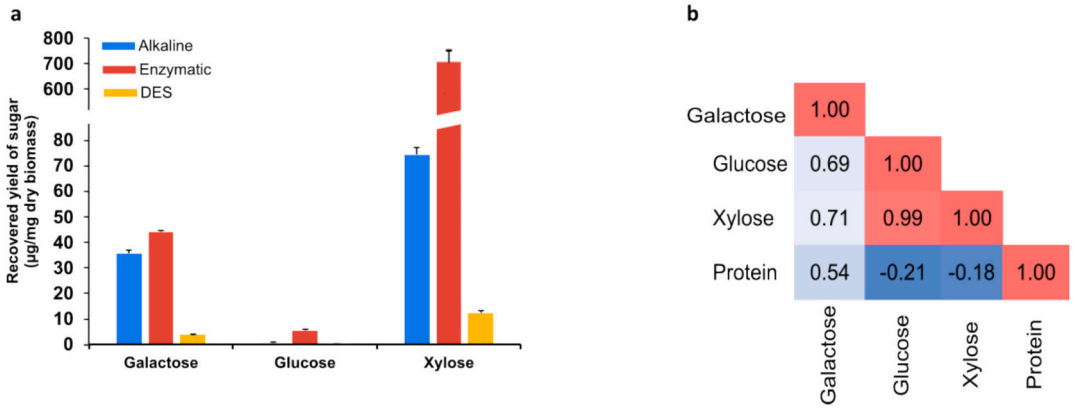

Fig. 5. (a) Extracted carbohydrates. (b) Pearson correlation of extracted carbohydrates and protein. Pearson's correlation range > 0.75 (high correlation), 0.3–0.75 (medium correlation), < 0.3 (low/no correlation). Negative/Positive values indicated the direction of correlation.

μg/mg) and glucose (5 μg/mg), consistent with effective hydrolysis of hemicellulosic xylan. However, the substantial sugar release did not translate into high protein recovery. This suggests that even when the cell wall is partially hydrolyzed, protein becomes trapped in the densely packed cortical tissues, and limited solvent penetration prevents its release. Buffer conditions used to maintain enzyme stability may further reduce protein denaturation and solubilization (Houser, Kosourova, Kubickova, & Wimmerova, 2021; Skehel, 2004).

Furthermore, xylanases predominantly hydrolyze β-(1,4)-xylose (Ye & Zhong, 2022), which may limit activity toward the β-(1,3)/β-(1,4)-mixed xylan in *P. palmata*. A newly identified marine xylanase capable of hydrolyzing both linkage types has recently been reported (Zhao et al., 2023), highlighting the potential importance of enzyme specificity for targeting mixed-linkage xylans. Nevertheless, the impact of this enzymatic specificity on protein recovery from *P. palmata* requires further investigation. Additionally, because phycoerythrin is a large, multimeric 240–250 kDa protein (Chang et al., 1996), protease co-treatment (e.g., Alcalase) may be required to reduce protein size and increase solubility, as shown in previous work yielding 50–55% protein recovery (Ghelichi, Sørensen, Hajfathalian, Holdt, & Jacobsen, 2025; Naseri et al., 2020).

In alkaline extraction, sugar release was more moderate (74 μg/mg xylose, 35 μg/mg galactose, 0.44 μg/mg glucose). Protein extraction under alkaline conditions is thus driven more strongly by protein solubilization and peptide cleavage, rather than the extent of cell wall degradation (Din et al., 2023; Hadidi et al., 2023).

DES extraction released very small amounts of sugar, consistent with limited cell wall modification and the lowest protein recovery, which may reflect insufficient DES-cell wall interaction. Mechanical enhancement (e.g., bead milling) has been shown to improve solvent penetration in IL/DES extraction systems (Garcia et al., 2023).

Fig. 5b revealed low correlation between protein recovery and glucose or xylose release, while galactose showed a moderate correlation ($r = 0.54$). Galactose may originate from floridoside (Dussan et al., 2024) or from substitution on mixed-linkage xylan (Deniaud, Gall, Rusig, & Lahaye, 2006), but degradation of galactose-containing components alone does not guarantee improved protein recovery (Idowu et al., 2024).

Overall, these carbohydrate analyses indicate that protein extraction is not solely determined by cell wall hydrolysis. Instead, protein recovery yield is influenced by the synergistic interaction between cell wall modification, tissue architecture, and protein solubilization pathways. The sugar analysis and CFW staining analysis were used as proxy for structural modification/alteration and were not directly measuring protein accessibility or permeability. CFW staining primarily reflects changes in β-glucan exposure and overall wall integrity, while monosaccharide release indicates polysaccharide solubilization rather than actual protein diffusion or extraction efficiency.

Previous studies on *P. palmata* have mainly focused on optimizing biochemical extraction conditions (Bjarnadóttir et al., 2018; Harnedy & FitzGerald, 2013; Naseri et al., 2020); with microscopy used primarily to confirm cell wall disruption as the key mechanism enhancing protein yield (Wijethunga et al., 2025). In contrast, our results show that extraction efficiency is not governed solely by cell wall breakdown. We identified that dense cortical tissue imposes constraints on solvent penetration and protein mass transfer, where tightly packed cells and limited intercellular space act as physical diffusion barriers. Importantly, cellular architecture is not the sole limiting factor; rather, cell density, the degree cell wall breakdown, and protein solubilization operate as complementary and non-interchangeable mechanisms that collectively govern the extraction process. This structural perspective represents the key novelty of this study, extending existing work beyond biochemical optimization by demonstrating that internal tissue organization critically limits protein extraction from *P. palmata*.

4. Perspective

The present study demonstrates that the majority of protein in *P. palmata* is localized within the small, densely packed cells of the cortical region, which forms a structural barrier to solvent penetration during extraction. This tissue organization restricts the accessibility of extraction agents and limits the transfer of intracellular proteins into solution. While alkaline extraction showed the highest protein recovery yield, it did not fully overcome the resistance of the compact cortex. Therefore, improving protein accessibility will require approaches that specifically address the morphological constraints of the thallus.

Future work should focus on developing strategies that enhance solvent penetration and weaken the cell–cell connectivity in the cortex. Mechanical disruption (e.g., bead milling, pulsed-pressure treatment, microfluidization) may be necessary prior to extraction to enhance solvent penetration and expose the cytoplasmic protein pool. We hypothesize that mechanical pre-treatments will exhibit a non-linear relationship with protein recovery, where moderate disruption maximizes extractability, while excessive mechanical pre-treatment at a certain point no longer increases protein recovery yield. This phenomenon was e.g. observed during a co-extraction process using ionic liquids and bead milling for protein extraction from *Ulva,* where harsh treatment induced protein aggregation, thereby decreasing protein solubility and reducing extraction yield (Garcia et al., 2023). As different seaweeds vary in morphology and composition, the effect of mechanical pretreatment on protein extraction yield may differ.

Optimization of cultivation strategies, such as adjusting nutrient availability or harvesting stage, may reduce cell wall thickness and tissue density, thereby increasing extractability. A testable hypothesis arising from this work is that *P. palmata* harvested at earlier growth

stages, when cortical cells are less densely packed, will yield higher protein recoveries under identical extraction conditions. This is supported by previous findings showing that carrageenan extraction efficiency is influenced by the cultivation duration of *Kappaphycus alvarezii* biomass (Periyasamy, Subba Rao, & Anantharaman, 2018; Subramaniam, Surugau, Aziz, Shukri, & Muhammad, 2023). Therefore, integrating upstream cultivation control with downstream extraction design may ultimately unlock the full potential of *P. palmata* as a sustainable protein source.

5. Conclusion

This study provides the first detailed structural analysis for the limited protein recovery yields observed from *P. palmata*. The dense tissue organization of the cortical region, characterized by tightly packed small cells with minimal intercellular space, forms a natural barrier to mass transfer during extraction. Consequently, solvent penetration and protein solubilization are constrained, even when the chemical or enzymatic treatments partially disrupt the cell wall.

Among the treatments tested, alkaline extraction achieved the highest protein recovery yield (~60%), which is attributed to both moderate disruption of cell wall and the hydrolysis of intracellular proteins into smaller, more soluble fragments. In contrast, xylanase-assisted extraction resulted in the most severe cell wall degradation but yielded only ~27% solubilized protein, indicating that cell wall hydrolysis alone does not guarantee protein release from densely packed tissues. DES-assisted extraction resulted in the lowest protein recovery (~14%) and showed minimal effects on cell wall or tissue architecture. None of the extraction strategies significantly altered the intrinsic tissue density of the cortex.

Taken together, these findings show that protein recovery from *P. palmata* is not solely governed by cell wall degradation but is strongly limited by thallus architecture. Therefore, improving extraction efficiency will require combining biochemical extraction approaches with mechanical pre-disruption and potentially enzyme cocktails that include both xylanases targeting β-(1,3)/β-(1,4)-xylan linkages and proteases capable of partially fragmenting large phycobiliproteins. Such integrated strategies are likely necessary to overcome the structural constraints imposed by dense cortical tissue and thus to improve protein isolation from seaweed.

Declaration of generative AI use

During the preparation of this manuscript, the authors used ChatGPT (OpenAI) to assist with grammar correction and language refinement. After using this tool, the corresponding author reviewed and edited the content to ensure accuracy and clarity and took full responsibility for the final version of the manuscript.

CRediT authorship contribution statement

Agusman Agusman: Writing – original draft, Methodology, Investigation, Formal analysis, Data curation, Conceptualization. **Wouter J.J. Huijgen:** Writing – review & editing. **Michel H.M. Eppink:** Writing – review & editing. **Rene H. Wijffels:** Writing – review & editing. **Norbert C.A. de Ruijter:** Writing – review & editing, Methodology, Investigation, Data curation. **Antoinette Kazbar:** Writing – review & editing, Validation, Supervision, Project administration, Methodology, Funding acquisition, Conceptualization.

Declaration of competing interest

The authors declare that they have no known competing financial interests or personal relationships that could have appeared to influence the work reported in this paper.

Acknowledgement

This research was supported by the LPDP Scholarship of A.A. from the Government of the Republic of Indonesia. The authors thank Hortimare for providing biomass. The authors thank Wageningen Light Microscopy Centre (WLMC) for providing training and facilities for sample preparation and microscopy. W.H. acknowledges Cosun RD&I for supporting his position at Wageningen University & Research.

Appendix A. Supplementary data

Supplementary data to this article can be found online at https://doi.org/10.1016/j.foodchem.2026.149680.

Data availability

No data was used for the research described in the article.

References

Aasen, I. M., Sandbakken, I. S., Toldnes, B., Roleda, M. Y., & Slizyte, R. (2022). Enrichment of the protein content of the macroalgae Saccharina latissima and Palmaria palmata. *Algal Research, 65*. https://doi.org/10.1016/j.algal.2022.102727

Aslam, S., Akhtar, A., Nazir, W., Khalid, N., & Barrow, C. J. (2024). Downstream processing, functional properties, and applications of extracted proteins from nonconventional sources for improving food sustainability. ACS Food Science and Technology, 18;4(10):2301–21. Doi: https://doi.org/10.1021/acsfoodscitech.4c00418.

Baweja, P., Kumar, S., Sahoo, D., & Levine, I. (2016). Chapter 3 - biology of seaweeds. In J. Fleurence, & I. Levine (Eds.), *Seaweed in health and disease prevention* (pp. 41–106). San Diego: Academic Press.

Bjarnadóttir, M., Aðalbjörnsson, B. V., Nilsson, A., Slizyte, R., Roleda, M. Y., & Hreggviðsson, G.Ó. (2018). Palmaria palmata as an alternative protein source: Enzymatic protein extraction, amino acid composition, and nitrogen-to-protein conversion factor. *Journal of Applied Phycology*. https://doi.org/10.1007/s10811-017-1351-8

Bojorges, H., López-Rubio, A., Martínez-Abad, A., & Fabra, M. J. (2023). Overview of alginate extraction processes: Impact on alginate molecular structure and techno-functional properties. *Trends in Food Science & Technology, 140*. https://doi.org/10.1016/j.tifs.2023.104142

Bouzon, Z. L., Simioni, C., & Schmidt, E. C. (2014). The structure and morphology of red algae chloroplasts. In M. F. Hohmann-Marriott (Ed.), *The structural basis of biological energy generation* (pp. 295–308). Dordrecht: Springer Netherlands.

Brglez Mojzer, E., Knez Hrnčič, M., Škerget, M., Knez, Ž., & Bren, U. (2016). Polyphenols: Extraction methods, Antioxidative action, bioavailability and Anticarcinogenic effects. *Molecules, 21*.

Deniaud, E., Gall, L., Rusig, A., & Lahaye, M. (2006). Initial observations on glycoside deposition in cell walls of Palmaria palmata (L.) Kuntze (Rhodophyta) during spore germination. Botanica Marina - BOT MAR, 49, 266–269. Doi: 10.1515/BOT.2006.031.

Deniaud, E., Quemener, B., Fleurence, J., & Lahaye, M. (2003). Structural studies of the mix-linked β-(1→3)/β-(1→4)-d-xylans from the cell wall of Palmaria palmata (Rhodophyta). International Journal of Biological Macromolecules(v;33(1–3):9–18). Doi: https://doi.org/10.1016/S0141-8130(03)00058-8.

Din, W. H. M., Chen, C. W., Huang, C. Y., Singhania, R. R., Sung, Y. J., & Dong, C. D. (2023). Development of bioactive peptides derived from red algae for dermal care applications: Recent advances. *Sustainability, 15*(11), Article 8506.

Dussan, K., Huijgen, W. J. J., de Vrije, T., van der Wal, H., Capella, H., van Doorn, J., & van Hal, J. W. (2024). Biorefinery of red seaweed Palmaria palmata for production of bio-based chemicals and biofuels. *Algal Research, 82*. https://doi.org/10.1016/j.algal.2024.103608

Fleurence, J., Massiani, L., Guyader, O., & Mabeau, S. (1995). Use of enzymatic cell wall degradation for improvement of protein extraction from Chondrus crispus, Gracilaria verrucosa and Palmaria palmata. Journal of Applied Phycology, 1;7(4):393–7. Doi: doi.org/https://doi.org/10.1007/BF00003796.

Garbary, D. J., & Kim, K. Y. (2005). Anatomical differentiation and photosynthetic adaptation in brown algae. *Algae, 20*(3), 233–238. https://doi.org/10.4490/algae.2005.20.3.233

Garcia, S. E., Miranda, C. F., Cesario, M. T., Wijffels, R. H., van den Berg, C., & Eppink, M. H. M. (2023). Ionic liquid-assisted selective extraction and partitioning of biomolecules from macroalgae. *ACS Sustainable Chemistry & Engineering, 11*(5), 1752–1762. https://doi.org/10.1021/acssuschemeng.2c05823

Ghelichi, S., Sørensen, A.-D. M., Hajfathalian, M., Holdt, S. L., & Jacobsen, C. (2025). Screening enzymatic extracts of Palmaria palmata based on composition and bioactivity. *Algal Research, 89*. https://doi.org/10.1016/j.algal.2025.104048

Hadidi, M., Aghababaei, F., & McClements, D. J. (2023). Enhanced alkaline extraction techniques for isolating and modifying plant-based proteins. *Food Hydrocolloids, 145*. https://doi.org/10.1016/j.foodhyd.2023.109132

Harnedy, P. A., & FitzGerald, R. J. (2013). Extraction of protein from the macroalga Palmaria palmata. *LWT - Food Science and Technology, 51*(1), 375–382. https://doi.org/10.1016/j.lwt.2012.09.023

Hernández-Corroto, E., Olivares-Galván, S., Marina, M. L., & García, M. C. (2023). Approaching the extraction of proteins from brewing wastes using deep eutectic solvents. *Lwt*. https://doi.org/10.1016/j.lwt.2023.115470

Houser, J., Kosourova, J., Kubickova, M., & Wimmerova, M. (2021). Development of 48-condition buffer screen for protein stability assessment. *European Biophysics Journal, 50*(3), 461–471. https://doi.org/10.1007/s00249-021-01497-6

Idowu, A. T., Amigo-Benavent, M., & FitzGerald, R. J. (2024). Impact of alkaline solution, carbohydrase and biomass:Solvent on extraction efficiency, and protein and amino acid profiles of Palmaria palmata protein extracts. *Food and Bioproducts Processing, 148*, 285–297. https://doi.org/10.1016/j.fbp.2024.09.017

Janke, L. (2024). Mapping the global mass flow of seaweed: Cultivation to industry application. *Journal of Industrial Ecology, 28*(5), 1256–1269. https://doi.org/10.1111/jiec.13539

Chang, W.-R., Jiang, T., Wan, Z.-l., Zhang, J.-p., Yang, Z.-x., & Liang, D.-c. (1996). Crystal structure of R-phycoerythrin from Polysiphonia urceolata at 2.8 Å resolution. Journal of Molecular Biology, 262(5), 721–722. Doi: Doi: https://doi.org/10.1006/jmbi.1996.0547.

Juul, L., Haue, S. K., Bruhn, A., Boderskov, T., & Kastrup Dalsgaard, T. (2023). Alkaline pH increases protein extraction yield and solubility of the extracted protein from sugar kelp (Saccharina latissima). *Food and Bioproducts Processing, 140*, 144–150. https://doi.org/10.1016/j.fbp.2023.05.008

Karina, H.-C., Cristian, J.-M., Madeleine, P.-A., Elena, M. C. L., Perea-Flores, M.d. J., Gustavo Fidel, G.-L., & Gloria, D.-O. (2022). Chemical and microstructural characterization of three seaweed species from two locations of Veracruz, Mexico. *Food Science and Technology, 42*. https://doi.org/10.1590/fst.41421

Kaur, C., Singh, A., Sethi, M., Devi, V., Chaudhary, D. P., Phagna, R. K., … Rakshit, S. (2022). Optimization of protein quality assay in normal, opaque-2, and quality protein maize. *Frontiers in Sustainable Food Systems, 6*, Article 2022. https://doi.org/10.3389/fsufs.2022.743019

Kruger, N. J. (1994). The Bradford method for protein quantitation. *Methods in Molecular Biology, 32*, 9–15. https://doi.org/10.1385/0-89603-268-x:9

Lahaye, M., Michel, C., & Barry, J. L. (1993). Chemical, physicochemical and in-vitro fermentation characteristics of dietary fibres from Palmaria palmata (L.) Kuntze. *Food Chemistry, 47*(1), 29–36. https://doi.org/10.1016/0308-8146(93)90298-T

Liu, C., Gao, J., Jiang, H., Sun, J., Gao, X., & Mao, X. (2024). Value-added utilization technologies for seaweed processing waste in a circular economy: Developing a sustainable modern seaweed industry. *Comprehensive Reviews in Food Science and Food Safety, 23*(6). https://doi.org/10.1111/1541-4337.70027

Liu, C., Guo, B., Xia, Q., Meng, J., Chen, W., & Liu, S. (2017). Efficient cleavage of strong hydrogen bonds in cotton by deep eutectic solvents and facile fabrication of cellulose nanocrystals in high yields. ACS Sustainable Chemistry & Engineering, 5;5(9): 7623–31. Doi: https://doi.org/10.1021/acssuschemeng.7b00954.

Lüder, U., Knoetzel, J., & Wiencke, C. (2001). Acclimation of photosynthesis and pigments to seasonally changing light conditions in the endemic Antarctic red macroalga Palmaria decipiens. *Polar Biology, 24*(8), 598–603. https://doi.org/10.1007/s003000100260

Machu, L., Misurcova, L., Ambrozova, J. V., Orsavova, J., Mlcek, J., & Sochor, J. (2015). Phenolic content and antioxidant capacity in algal food products. Molecules, 12;20 (1):1118–33. Doi: doi.org/https://doi.org/10.3390/molecules20011118.

Mæhre, H., Jensen, I.-J., & Eilertsen, K.-E. (2016). Enzymatic pre-treatment increases the protein bioaccessibility and extractability in Dulse (Palmaria palmata). *Marine Drugs, 14*(11), 196. https://doi.org/10.3390/md14110196

Matsushima, R. (2014). Thin sections of Technovit 7100 resin of Rice endosperm and staining. *Bio-Protocol, 4*(18). https://doi.org/10.21769/bioprotoc.1239

Moldes, D., Requejo, P. F., Vega, M., Bolado, S., Wijffels, R. H., & Kazbar, A. (2024). Protein extraction from seaweed Saccharina latissima with deep eutectic solvents. *Microchemical Journal, 205*. https://doi.org/10.1016/j.microc.2024.111275

Naseri, A., Marinho, G. S., Holdt, S. L., Bartela, J. M., & Jacobsen, C. (2020). Enzyme-assisted extraction and characterization of protein from red seaweed Palmaria palmata. Algal Research, 47(April 2019), 101849–101849. Doi: https://doi.org/10.1016/j.algal.2020.101849.

Noble, J. E., & Bailey, M. J. (2009). Quantitation of protein. *Methods in Enzymology, 463*, 73–95. https://doi.org/10.1016/s0076-6879(09)63008-1

Periyasamy, C., Subba Rao, P. V., & Anantharaman, P. (2018). Harvest optimization to assess sustainable growth and carrageenan yield of cultivated Kappaphycus alvarezii (Doty) Doty in Indian waters. *Journal of Applied Phycology, 31*(1), 587–597. https://doi.org/10.1007/s10811-018-1562-7

Piccinini, L., Nirina Ramamonjy, F., & Ursache, R. (2024). Imaging plant cell walls using fluorescent stains: The beauty is in the details. *Journal of Microscopy, 295*(2), 102–120. https://doi.org/10.1111/jmi.13289

Ramus, J., Beale, S. I., Mauzerall, D., & Howard, K. L. (1976). Changes in photosynthetic pigment concentration in seaweeds as a function of water depth. *Marine Biology, 37* (3), 223–229. https://doi.org/10.1007/BF00387607

Sabeena, F. K., & Jacobsen, C. (2013). Phenolic compounds and antioxidant activities of selected species of seaweeds from Danish coast. Food Chemistry, 1;138(2–3): 1670–81. Doi: https://doi.org/10.1016/j.foodchem.2012.10.078.

Sanchez, A., Guzman, A., Ortiz, A., Rembao, D., Espinosa, B., Zenteno, E., & Guevara, J. (2001). Toluidine blue-O staining of prion protein deposits. *Histochemistry and Cell Biology, 116*(6), 519–524. https://doi.org/10.1007/s00418-001-0343-5

Sasaki, T., & Matsui, S. (1972). Effect of acetic acid concentration on the color reaction in the o-toluidine-boric acid method for blood glucose estimation. *Japanese Journal of Clinical Chemistry, 1*(3), 346–353. https://doi.org/10.14921/jscc1971b.1.3_346

Shawky, E., Zhu, W., & Tian, J. (2025). A review of innovative extraction technologies for protein recovery from plant-based by-products: A step toward zero-waste processing. *International Journal of Biological Macromolecules, 315*, Article 144301. https://doi.org/10.1016/j.ijbiomac.2025.144301

Skehel, J. M. (2004). Preparation of extracts from animal tissues. In P. Cutler (Ed.), *Protein purification protocols* (pp. 15–20). Totowa, NJ: Humana Press.

Sridharan, G., & Shankar, A. A. (2012). Toluidine blue: A review of its chemistry and clinical utility. *J Oral Maxillofac Pathol, 16*(2), 251–255. https://doi.org/10.4103/0973-029X.99081

Subramaniam, G., Surugau, N., Aziz, N. A. A., Shukri, R., & Muhammad, K. (2023). The effects of cultivation type and maturity stage on arsenic species concentration and carrageenan content in Kappaphycus spp. from Semporna, Sabah. *Journal of Applied Phycology, 35*(5), 2383–2395. https://doi.org/10.1007/s10811-023-03021-z

Vilg, J. V., & Undeland, I. (2017). pH-driven solubilization and isoelectric precipitation of proteins from the brown seaweed Saccharina latissima-effects of osmotic shock, water volume and temperature. *Journal of Applied Phycology, 29*(1), 585–593. https://doi.org/10.1007/s10811-016-0957-6

VilgyarisVan Wychen, S., & Laurens, L. M. L. (2023). *Determination of Total carbohydrates in algal biomass: Laboratory analytical procedure (LAP)*. Golden, CO: National Renewable Energy Laboratory.

Wang, L., Li, G., Chen, X., Yang, Y., Liew, R. K., Abo-Dief, H. M., & Li, H. (2024). Extraction strategies for lignin, cellulose, and hemicellulose to obtain valuable products from biomass. *Advanced Composites and Hybrid Materials, 7*(6). https://doi.org/10.1007/s42114-024-01009-y

Wang, L., Wang, L., Liu, X., Lin, X., Fei, T., & Zhang, W. (2025). Seaweeds-derived proteins and peptides: Preparation, virtual screening, health-promoting effects, and industry applications. Critical Reviews in Food Science and Nutrition, 0(0), 1–28. Doi: https://doi.org/10.1080/10408398.2025.2449596.

Wijethunga, A. M., He, Q. S., Prithiviraj, B., & Sun, X. (2025). Acid hydrolysis and microwave digestion enhanced protein extraction from red seaweed Palmaria palmata. *Food Chem X, 25*, Article 102222. https://doi.org/10.1016/j.fochx.2025.102222

Yadav, M., & Singh, Y. (2020). The solvent mediated interaction potential between solute particles: Theory and applications. *Soft Matter, 16*(42), 9780–9788. https://doi.org/10.1039/d0sm01168a

Yarish, C., Brummett, R., Hansen, S., Bjerregaard, R., Valderrama, D., & Sims, N. (2016). *Seaweed aquaculture for food security income generation and environmental health in tropical developing Countries*. World Bank.

Ye, Z. H., & Zhong, R. (2022). Outstanding questions on xylan biosynthesis. *Plant Science, 325*, Article 111476. https://doi.org/10.1016/j.plantsci.2022.111476

Zhang, B., Peng, Y., Rawiwan, P., Wheeler, T., Fitzgerald, J., Huffman, L., & Quek, S. Y. (2024). Effect of extraction processes on the physicochemical and functional properties of protein-rich extracts from the red seaweed Pyropia Seriata (nori). *Future Foods, 10*, Article 100501. https://doi.org/10.1016/j.fufo.2024.100501

Zhao, F., Wang, Z., & Huang, H. (2024). Physical cell disruption technologies for intracellular compound extraction from microorganisms. *Processes, 12*.

Zhao, F., Yu, C.-M., Sun, H.-N., Zhao, L.-S., Ding, H.-T., Cao, H.-Y., & Chen, X.-L. (2023). A novel class of xylanases specifically degrade marine red algal β1,3/1,4-mixed-linkage xylan. *Journal of Biological Chemistry, 299*(9), Article 105116. https://doi.org/10.1016/j.jbc.2023.105116